The Real Role of 4,4'-Bis[*N*-[4-{*N,N*-bis(3-methylphenyl)amino}phenyl]-*N*-phenylamino]biphenyl (DNTPD) Hole Injection Layer in OLED: Hole Retardation and Carrier Balancing[†]

Hyoung-Yun Oh, Insun Yoo,[‡] Young Mi Lee,[§] Jeong Won Kim,[§] Yeonjin Yi,[§] and Seonghoon Lee[*]

School of Chemistry, NS 60, Seoul National University, Seoul 151-747, Korea. [*]E-mail: shnlee@snu.ac.kr
[‡]LG Display R & D Center, 1007, Deongeun-ri, Wollong-myeon, Paju-si, Gyeonggi-do 413-811, Korea
[§]Division of Advanced Technology, Korea Research Institute of Standards and Science, Daejeon 305-340, Korea

We explored interfacial electronic structures in indium tin oxide (ITO)/DNTPD/*N,N'*-diphenyl-*N,N'*-bis(1-naphthyl)-1,1'-biphenyl-4,4'-diamine (NPB) layer stack in an OLED to clarify the real role of an aromatic amine-based hole injection layer, DNTPD. A hole injection barrier at the ITO/DNTPD interface is lowered by 0.20 eV but a new hole barrier of 0.36 eV at the DNTPD/NPB is created. The new barrier at the DNTPD/NPB interface and its higher bulk resistance serve as hole retardation, and thus those cause the operation voltage for the ITO/DNTPD/NPB to increase. However, it improves current efficiency through balancing holes and electrons in the emitting layer.

Key Words : OLED, DNTPD, NPB, UPS, Injection barrier

Introduction

After finding the double layered organic light emitting diode (OLED) by Tang and Van Slyke,[1] persistent progress in current efficiency and operational stability has been accomplished through adopting an additional hole injection layer (HIL) between an anode and a hole transport layer (HTL).[2] A hole barrier lowering at anode/organic interface and the formation of morphologically stable amorphous interface film on the anode have been thought as the important factors bringing the improvements in device performance. Accordingly, many kinds of aromatic amine derivatives[3-5] with relatively lower ionization energy (IE) than that of ITO and no light absorption in the visible range have been synthesized and applied to the OLEDs. Among them, 4,4',4''-tris[3-methyl-phenyl (phenyl) amino]-triphenylamine (MTDATA)[6-8] and *N,N'*-diphenyl-*N,N'*-bis-[4-(phenyl-m-tolyl-amino)-phenyl]-biphenyl-4,4'-diamine (DNTPD)[9-12] have shown proper optical properties and IE values (5.1 eV). The former has been frequently used in academic researches and the latter in commercial productions.[9,10] In spite of their important role in OLEDs, however, the origin of the improvements in device performance with such HILs has not ever been investigated and understood clearly. The interfacial electronic structures in the indium tin oxide (ITO)/ organic HIL/HTL layered stack may play a critical role in the improvement of device performance.

Current photoemission studies on metal/organic[13-16] or organic/organic interfaces[17-20] reveal that the interfacial barrier height estimated from the difference of separately observed IE values of thin films is far from the reality because the traditional vacuum level alignment is not always valid. In addition, Braun *et al.*[18] reported that the alignment of energy levels depended on the equilibration of the chemical potential throughout the layer stack and that the interfacial energy barrier between the highest occupied molecular orbital (HOMO) of MTDATA and that of 4,4'-*N,N'*-dicarbazolyl-bipheny (CBP) was significantly changed with respect to the work functions of the substrates contacting with MTDATA layer. From this standpoint of view, the investigation of the interfacial energy level alignments in ITO/HIL/HTL layer stack is worth doing to clarify interfacial electronic structures of the films and to construct the efficient device. To clarify the role of DNTPD, commercially promising material, as a HIL, we measured ultraviolet photoemission spectra (UPS) and fabricated the devices with DNTPD as a HIL.

Experimental

Commercially available DNTPD (CHEMIPRO KASEI KAISHA, Ltd.) and *N,N'*-diphenyl-*N,N'*-bis(1-naphthyl)-1, 1'-biphenyl-4,4'-diamine (NPB) were used as HIL and HTL, respectively. ITO-coated glass (hereafter ITO substrate) was used as a substrate both for the interface measurement and the fabricated device. The ITO substrates were cleaned in terms of the house cleaning procedure of sonication in a detergent and a rinse in deionized water followed by UV ozone treatment.

In situ UPS measurements were made to explore electronic structures at the DNTPD HIL interfaces and we obtained information on the vacuum level and a HOMO energy level. DNTPD and NPB were thermally evaporated onto an ITO-coated glass substrate (hereafter ITO substrate) in a deposition

---

chamber maintained below 5×10^{-9} Torr. The deposition rates of both DNTPD and NPB were controlled to be 1 Å/s, monitored by a quartz crystal microbalance. To investigate the interface between them, DNTPD (20 nm) and NPB (20 nm) were deposited onto an ITO substrate in a stepwise manner. Before and after each deposition step, the sample was transferred to an analysis chamber and measured without the vacuum interruption. The analysis chamber was composed of a hemispherical electron energy analyzer (VG ESCA LAB 220i) and a UV (He I, 21.22 eV) discharge source. The UPS spectra were obtained with a sample bias of −10 V in a normal emission geometry to measure the secondary electron cutoff. We also prepared an ITO/NPB layer stack film as a control sample and carried out similar measurements. The secondary electron cutoff and the HOMO onset positions were estimated with the line fitting as shown in Figure 1. The energy scale of presented spectra was calibrated with respect to the Fermi level of the sputter-cleaned Au substrate. To confirm the correlation of interfacial electronic structures with device performance, we made hole-only devices with ITO/NPB (100 nm)/Al, ITO/DNTPD (100 nm)/Al, and ITO/DNTPD (50 nm)/NPB (50 nm)/Al layer structures. Each organic material was thermally deposited

with 1 Å/s rate in a separate deposition chamber connected to a glove box. After evaporating 50 nm-thick Al as a cathode, all the devices were encapsulated with a 1-mm-thick glass cover containing a humidity absorber (Dynic). The current (*I*)-voltage (*V*) characteristic was measured by source-measure-units (SMU, Keithley 2400). The off-current levels of the devices were around 10^{-9} A.

Results and Discussion

The UPS spectra of the samples are shown in Figure 1 where the secondary cutoffs are shown in (a) and (b), and the HOMO positions from the Fermi energy are shown in (c) and (d). The (a) and (c) show the spectra with NPB deposited on bare ITO while (b) and (d) are obtained with the DNTPD HIL layer inserted between ITO and NPB. For both cases, the secondary electron cutoff positions were shifted toward to the higher binding energy compared with that of bare ITO. However, the total shift of the cutoff position of NPB toward higher binding energy is 0.12 eV as shown in (a), while that of DNTPD is 0.25 eV as shown in (b). An additional shift of 0.09 eV is observed after depositing the NPB layer on DNTPD as shown in (b). The shift of the
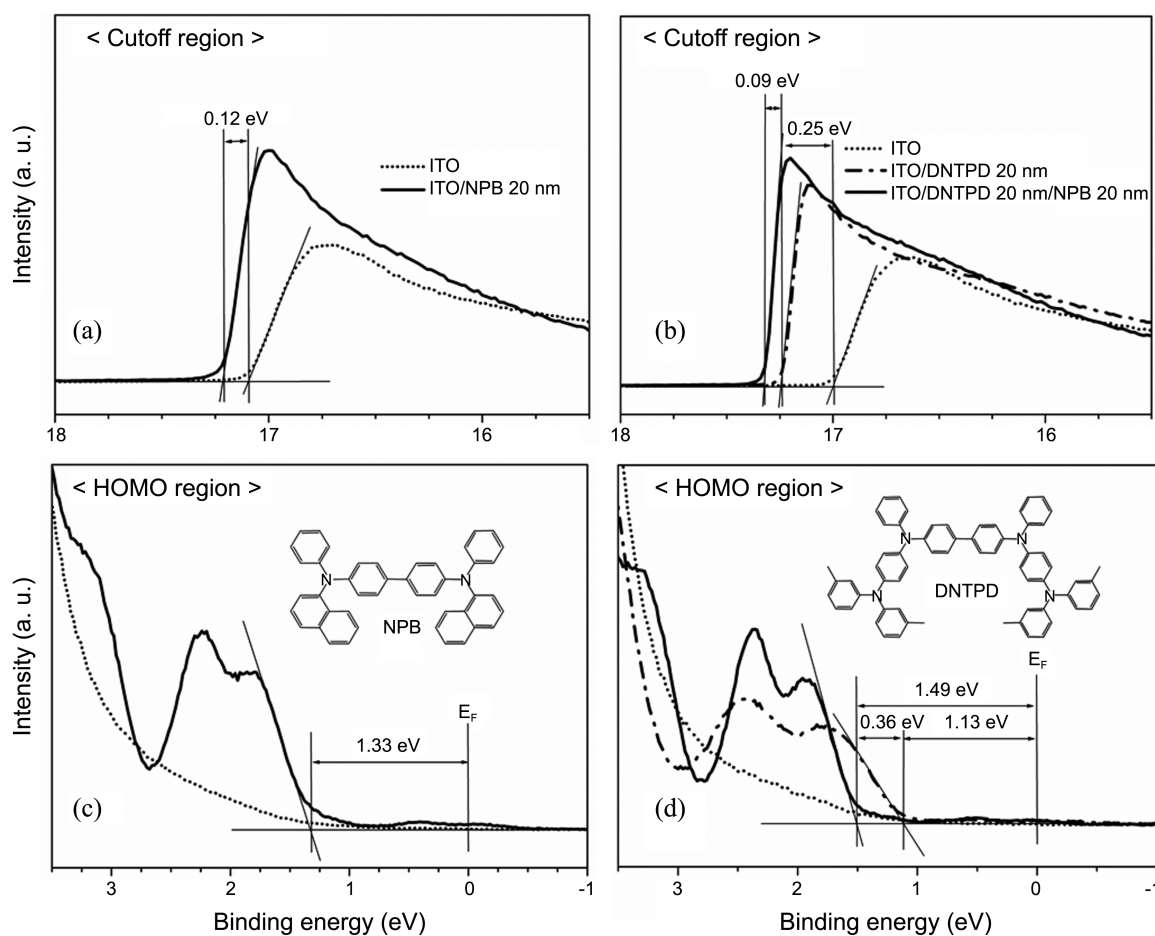
Figure 1. The measured UPS spectra of the samples. The secondary electron cutoff regions of (a) ITO/NPB and (b) ITO/DNTPD/NPB, respectively. The HOMO regions of (c) ITO/NPB and (d) ITO/DNTPD/NPB, respectively. The fitting procedure for determining the secondary electron cutoff and HOMO onset is indicated. The insets of (c) and (d) show chemical structures of NPB and DNTPD molecules, respectively.
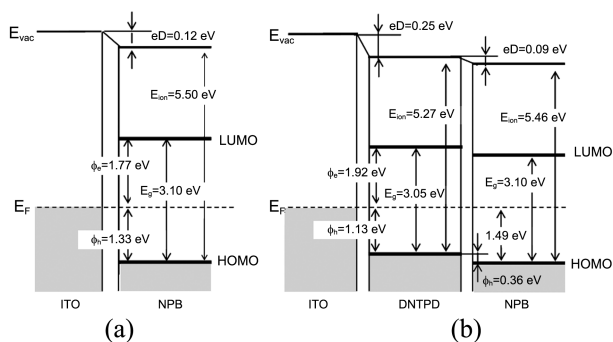
secondary cutoff position is attributed to the formation of interface dipoles due to the charge transfers between them.[13,20] The larger cutoff shift in DNPTD than in NPB reflects that ITO/DNPTD layer stack has larger interface dipoles with a negative pole pointing toward ITO than the ITO/NPB layer stack. Figure 1(c) and (d) show the HOMO region spectra of the samples. The HOMO onsets of the NPB and the DNTPD layer deposited on ITO are 1.33 eV and 1.13 eV, respectively.
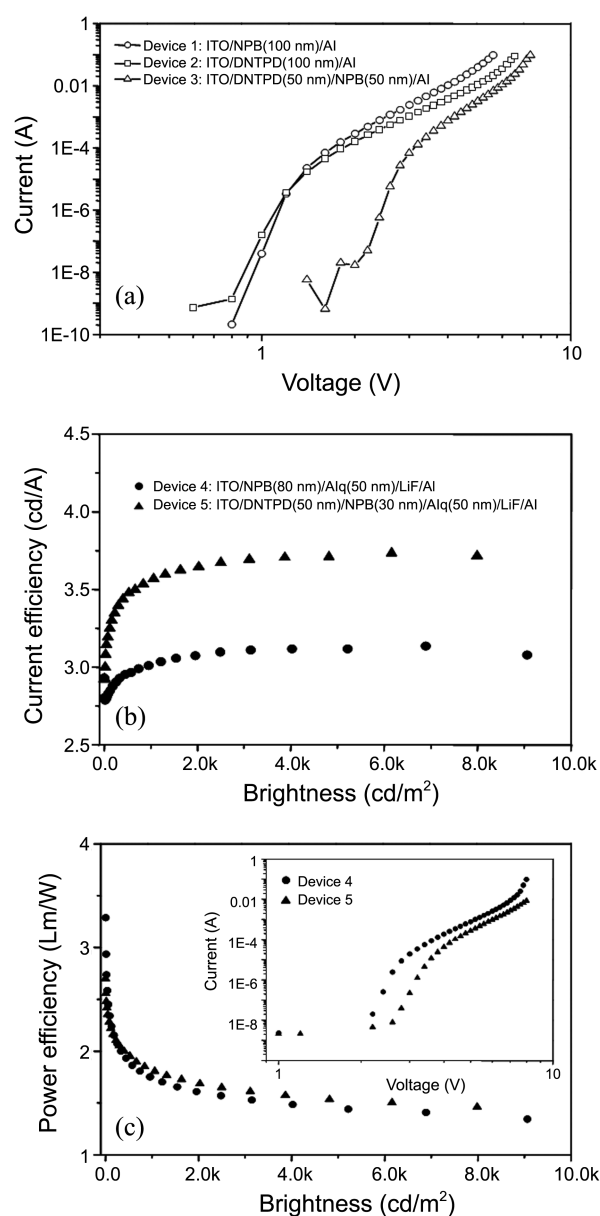
In the case of the NPB layer deposited on the DNTPD layer, the HOMO onset of the NPB is observed to be 1.49 eV. With information on HOMOs and vacuum levels, we draw the energy level diagrams of ITO/NPB and ITO/DNTPD/NPB layer stacks which are shown in Figure 2(a) and (b). The positions of the lowest unoccupied molecular orbitals (LUMO) of each material are estimated from the optical band gap determined from the absorption onset of the spectra (data not shown). The IEs of DNTPD and NPB are 5.27 eV and 5.46 eV, respectively. These values are good agreements with previous results within the error margin (0.05-0.1 eV) of UPS measurements.[16,21] Hole injection barriers from ITO to organic layers are 1.33 eV at ITO/NPB interface and 1.13 eV at ITO/DNTPD interface.

In a ITO/DNTPD/NPB layer stack (*i.e.* after depositing NPB on the DNTPD surface), however, another hole barrier between DNTPD and NPB exists and its value is 0.36 eV. That is, the DNTPD layer reduced a hole injection barrier by 0.20 eV at the ITO/DNTPD interface and formed a new hole barrier by 0.36 eV at the DNTPD/NPB interface. Accordingly, with the introduction of the hole injection layer of DNTPD in an OLED, we facilitate the hole injection from the ITO but this improvement is offset by the additional hole barrier existing between DNTPD and the NPB hole transporting layer.

To confirm the correlation of interfacial electronic structures with device performance, hole only devices with ITO/NPB (100 nm)/Al, ITO/DNTPD (100 nm)/Al, and ITO/DNTPD (50 nm)/NPB (50 nm)/Al layer structures (hereafter, Device 1, Device 2, and Device 3, respectively) were made. The current (I)-voltage (V) characteristic was shown in Figure 3(a). The required driving voltages of device 1, 2, and 3 at 5×10^{-8} A are 0.99, 0.92, and 2.15 V, respectively. Device 2

Figure 3. (a) *I-V* properties of hole only devices, (b) and (c) current efficiencies and power efficiency, respectively, as a function of brightness of light emitting devices. The inset in (c) shows *I-V* properties of the device 4, 5; all the pixel size is 2 mm × 2 mm.

with the lowest turn-on voltage indicates that the hole injection barrier of device 2 is lower than that of device 1 by approximately 0.1 V, which is in a good agreement with the observed difference in hole injection barrier (0.2 eV) as shown in Figure 2.

With an increasing driving voltage, device 1 shows much higher current density than those of the other devices because of its lower bulk resistance. In the case of device 3, both the additional hole barrier existing between DNTPD and NPB and the high bulk resistance play crucial roles in increasing its operation voltage. These results reflect that, even though the DNTPD layer reduces a hole injection barrier at the ITO interface by 0.20 eV, it, rather, works as hole retardation layer because of the additional hole barrier by 0.36 eV at the

Figure 2. Energy level diagrams of (a) ITO/NPB and (b) ITO/DNTPD/NPB structures. Φ_e and Φ_h are the electron and hole injection barrier. E_{ion} and eD are the ionization energy and an interface dipole.

DNTPD/NPB interface and its higher bulk resistance. Considering that the hole mobility in an OLED is usually much higher than that of the electron mobility under the same electric field,[22,23] the dramatic improvement of current efficiency in device 5 can be attributed to charge balancing[8] which results from the hole retardation due to the additional hole barrier and the high bulk resistance. This charge balancing is achieved by the introduction of the DNTPD as a hole injection layer (HIL). This can be demonstrated by fabricating a full OLED which has ITO/DNTPD interface at a proper position. We fabricated other devices, 4 and 5. Figure 3(b) shows the improvement of current efficiency in an organic light emitting device constructed by introducing a DNTPD hole injection layer between ITO and NPB layer. The current efficiency of device 5 with the structure of ITO/DNTPD (50 nm)/NPB (30 nm)/Alq$_3$ (50nm)/LiF (0.5 nm)/Al is enhanced more than 18% in the range over 1000 cd/m^2 than that of device 4 with the structure of ITO/NPB (80 nm)/Alq$_3$ (50 nm)/LiF (0.5 nm)/Al. In detail, the voltage increase of the device 5 is observed about 0.8 V at 0.5 mA (12 mA/cm^2) and 1 V at 5 mA (130 mA/cm^2) in comparison with the device 4. However, the improved current efficiency fully compensates it and therefore the power efficiency of the device 5 is slightly higher (Fig. 3(c)). Moreover, when we measured the operating hours of the devices (*i.e.*, its performance falling down to the 40% of the full light emission at 3000 cd/m^2), the devices 4 and 5 show 10 h, and 25 h, respectively. This lifetime improvement is due to the lower current density of device 5 for the same brightness, which is obtained by efficient charge balancing through inserting the DNTPD hole injection layer.

Conclusion

In summary, we investigated the real role of an aromatic amine-based hole injection layer (HIL) in an OLED by exploring interfacial electronic structures in the ITO/DNTPD/NPB layer stack. The DNTPD layer reduces a hole injection barrier by 0.20 eV at ITO/DNTPD interface, but creates a new hole barrier of 0.36 eV at the DNTPD/NPB interface. Therefore, even though the DNTPD layer reduces the hole injection barrier at the ITO interface, it, rather, works as a hole retardation layer because of the additional hole barrier at the DNTPD/NPB interface and its higher bulk resistance, and thus it causes the operation voltage for ITO/DNTPD/

NPB layer structures to increase. However, it helps the improvement in the current efficiency through balancing holes and electrons in the emitting layer of an OLED.

References

1. Tang, C. W.; Van Slyke, S. A. *Appl. Phys. Lett.* **1987**, *51*, 913.
2. Van Slyke, S. A.; Chen, C. H.; Tang, C. W. *Appl. Phys. Lett.* **1996**, *69*, 2160.
3. Shirota, Y.; Kageyama, H. *Chem. Phys.* **2007**, *107*, 953.
4. Sakai, T.; Hosokawa, C.; Kawamura, H.; Idemitsu Kosan Co., Ltd., *USP 6762438B2.*
5. Kido, J.; Fukoka, N.; Takeda, T. *JP08140960A.*
6. Shirota, Y.; Kuwabara, Y.; Inada, H.; Wakimoto, T.; Nakada, H.; Yonemoto, Y.; Kawami, S.; Imai, K. *Appl. Phys. Lett.* **1994**, *65*, 807.
7. Pfeiffer, M.; Forrest, S. R.; Leo, K.; Thompson, M. E. *Adv. Mater.* **2002**, *14*, 1633.
8. Wang, H.; Klubek, K. P.; Tang, C. W. *Appl. Phys. Lett.* **2008**, *93*, 93306.
9. Jung, S. O.; Kim, Y.-H.; Kwon, S.-K.; Oh, H.-Y.; Yang, J.-H. *Org. Electron.* **2007**, *8*, 349.
10. Yang, N. C.; Suh, M. C. *Curr. Appl. Phys.* **2009**, *9*, 505.
11. Jeon, W. S.; Park, T. J.; Park, J. J.; Kim, S. Y.; Jang, J.; Kwon, J. H.; Pode, R. *Appl. Phys. Lett.* **2008**, *92*, 113311.
12. Kim, S. H.; Jang, J.; Lee, J. Y. *Appl. Phys. Lett.* **2007**, *91*, 123509.
13. Crispin, X.; Geskin, V.; Crispin, A.; Cornil, J.; Lazzaroni, R.; Salaneck, W. R.; Brdas, J.-L. *J. Am. Chem. Soc.* **2002**, *124*, 8131.
14. Heimel, G.; Romaner, L.; Zojer, E.; Brdas, J.-L. *Nano Lett.* **2007**, *7*, 932.
15. Hill, I. G.; Kahn, A.; Soos, Z. G.; Pascal, R. A., Jr. *Chem. Phys. Lett.* **2000**, *327*, 181.
16. Lee, H.; Cho, S. W.; Han, K.; Jeon, P. E.; Whang, C.-N.; Jeong, K.; Cho, K.; Yi, Y. *Appl. Phys. Lett.* **2008**, *93*, 43308.
17. Ishii, H.; Sugiyama, K.; Ito, E.; Seki, K. *Adv. Mater.* **1999**, *11*, 605.
18. Braun, S.; de Jong, M. P.; Osikowicz, W.; Salaneck, W. R. *Appl. Phys. Lett.* **2007**, *91*, 202108.
19. Cho, S. W.; Yoo, K.-H.; Jeong, K.; Whang, C.-N.; Yi, Y.; Noh, M. *Appl. Phys. Lett.* **2007**, *91*, 52102.
20. Schlaf, R.; Parkinson, B. A.; Lee, P. A.; Nebesny, K. W.; Armstrong, N. R. *J. Phys. Chem. B* **1999**, *103*, 2984.
21. Chin, B. D. *J. Phys. D: Appl. Phys.* **2008**, *41*, 215104.
22. Chen, B. J.; Lai, W. Y.; Gao, Z. Q.; Lee, C. S.; Lee, S. T.; Gambling, W. A. *Appl. Phys. Lett.* **1999**, *75*, 4010.
23. Chu, T.-Y.; Song, O.-K. *Appl. Phys. Lett.* **2007**, *90*, 203512.